International Journal of Innovative Computing, Information and Control
Volume **19**, Number **3**, June **2023**

ICIC International ©2023 ISSN 1349-4198
pp. **805–819**

ANALYSIS OF HUMAN WALKING POSTURE USING A WEARABLE CAMERA

Ziyue Liu[1] and Joo Kooi Tan[2,*]

[1]Graduate School of Engineering
[2]Faculty of Engineering
Kyushu Institute of Technology
1-1, Sensui-cho, Tobata-ku, Kitakyushu-shi, Fukuoka 804-8550, Japan
liu.ziyue730@mail.kyutech.jp; *Corresponding author: etheltan@cntl.kyutech.ac.jp

Received November 2022; revised February 2023

Abstract. *In recent years, human posture has received widespread attention in the field of health promotion, and walking is one of the most popular exercises for keeping daily health. With respect to the walking posture of a person especially of the elderly, small changes in the posture have a great impact on their spine and lower limbs, resulting in changes in balance function. According to this fact, it is necessary to check human walking posture periodically. For this purpose, a simple, automatic way of examining a human walking posture is expected. This paper proposes a method of analyzing human walking motion: Two kinds of indicators about human walking posture are proposed which estimate posture changes from a camera worn by a person through changing scenery observed from the camera. In this method, AKAZE is applied to images to detect feature points and find their correspondences. A 5-point algorithm is used to estimate epipolar geometric constraints and provides an essential matrix for relative camera motion. Changes in the relative motion of the camera are used to analyze the changes of human walking posture. In the experiment, the characteristics of four types of walking postures (one is normal and the others are biased) were analyzed using the human posture indicators, and the reliability of the proposed method was verified.*

Keywords: Human walking motion, Wearable cameras, Walking motion analysis, Human posture indicators, Camera motion

1. **Introduction.** In recent years, human interests in maintaining and improving their health have increased greatly in the context of an aging society. Posture has been widely covered in various media, and even in the field of health promotion, posture is measured and exercises are provided based on their characteristics. In the background of this growing interest, in addition to aesthetic aspects such as beauty of posture, it is thought that there is a tendency to expect to prevent health damages caused by poor posture.

The word 'posture' refers to the posture or form of the body, but it can also be used metaphorically to refer to attitudes and mental attitudes. It can be said that this is because, since ancient times, people have treated the word 'posture' as being closely related not only to the posture of the body but also to the state of mind and spirit. Pleasure, happiness, and self-confidence are manifested in the dominant posture in the extended position, while unhappiness and inferiority complex are manifested in the dominant posture in the flexed position [1]. In addition, those with abnormal postures tend to be more depressed [2]. This suggests that the concept of posture indicates the physical and mental state, and that people have unconsciously placed importance on posture as a mirror that reflects their mind and body.

DOI: 10.24507/ijicic.19.03.805

An epidemiological survey reported that 61% of the elderly had a kyphotic posture. In this way, the elderly has a high proportion of kyphotic postures, and kyphotic deformity is one of the typical pathologies of the elderly. In addition, elderly people with kyphosis often experience arthralgia such as low back pain and knee joint pain and have difficulty walking due to fear of falling. In addition, they are dissatisfied with their kyphosis posture, which is reported to be accompanied by a decrease in opportunities to go out and a decline in QOL [3].

Walking is the most convenient means of transportation for humans. In recent years, attention has been focused on the presence of a natural trunk inclination during walking even in healthy adults [4]. However, the involvement of spine-pelvis posture and muscle activity in this case have not been investigated. A study of the walking posture of the elderly showed that a small change in posture has a large effect on the spine and lower limbs, resulting in a change in balance function [5]. Changes in the heavy trunk also affect the lower extremity joints during walking and movement [6]. Therefore, it is necessary to study the estimation and analysis of human walking posture. In this paper, we propose a method of estimating and analyzing one's walking posture from wearable camera images. The goal is to improve the walking posture by feeding back the analysis results to the person wearing the camera.

Human pose estimation, which has been developed for decades, aims to obtain the human pose from a given sensor input [7]. Vision-based approaches [8,9] are often used to provide such solutions by using cameras. There is a method called motion capture [10,11] that is used to create animation motion. In this method, multiple cameras are installed around a person, and his/her movements are photographed to create a 3D model. The system is large, because it requires multiple cameras and is heavy and time-consuming to install. Jiang and Tamagawa [12] performed a fall simulation using an open-source software called OpenSim. This research simply runs simulation, and it is necessary to create a human model by OpenSim. Earlier methods [13,14] employed probabilistic graphical models to represent the relationships between joints. Unfortunately, these methods parse a tree-structured state space into a lexicographic order based on image observation and human body topology, and rely heavily on handcrafted features, which limit their generalization and performance. More recently, there are methods [10,15,16] to detect the joint positions of pedestrians, such as attaching markers to pedestrians and estimating the pose by deep learning. Benenaula et al. [17] proposed a human pose estimation method using OpenPose and PoseNet. The results are chronologically analyzed by VGG19. This research requires the third viewpoint images from two cameras, limiting the observation as other existent methods, and performs gait classification using three neural networks.

In this paper, we propose a method of estimating walking posture of a person wearing a camera from frontal landscape images provided by the camera and analyzing the human body posture in the actual place instead of simulation, assuming daily walking support. We have developed two kinds of different techniques for obtaining self-posture using a wearable camera. One of the techniques is estimating self-posture using depth flow and motion network [18], in which the rotation angle of a wearable camera is estimated from the first view images using Depth and Motion Network and the other is estimating and decomposing camera motion (rotation) [9], in which 2D feature points are recovered to 3-D feature points using Epipolar geometry. The accuracy of the method is evaluated using a sensor giving the ground truth. In this paper, which is an extension of [9], the validity of the sensor as the ground truth and the effectiveness of the proposed method are verified. The human posture indicators are as well proposed to analyze various types of walking postures and they distinguish various walking postures effectively. Moreover, the technique is possible to determine walking posture anywhere, and to improve poor

walking posture, thereby maintaining human health and contributing to the realization of a safe and secure life.

The remainder of this paper is organized as follows. Section 2 provides an overview of the feature point extraction and feature point matching algorithms used in this study. Section 3 presents a method to estimate human walking posture based on the use of corresponding points. In Section 4, real human walking posture data are processed and analyzed. It is verified by experiments in Section 5. Performance of the proposed method is discussed in Section 6, and, finally, conclusion of this study is given in Section 7. Figure 1 shows the overall flow of the proposed method.

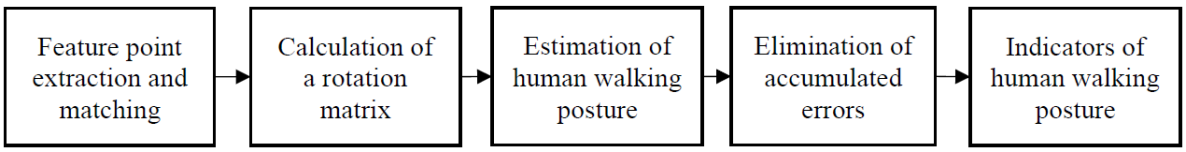

FIGURE 1. Overall flow of the proposed method

2. Feature Point Extraction and Matching.

2.1. **Feature point detection by AKAZE.** For feature point detection, Lowe [19] proposed a scale invariant feature transform (SIFT) matching algorithm. It constructs a scale space and extracts scale-invariant feature points. Aiming at solving the shortcomings of speed and computational complexity of SIFT, Bay et al. [20] proposed a speeded-up robust features algorithm (SURF). It improves the efficiency of feature matching by using the approximate Harr wavelet algorithm to extract the feature points. However, the Gaussian scale space constructed by these two methods is easy to ignore the edge detail information of the image. Alcantarilla et al. [21] preserved the edge information of images by using nonlinear diffusion to describe features in nonlinear scale space, and proposed a new 2D feature extraction method, namely AKAZE. The method proposed in this paper analyzes human walking posture by video. It is done by extracting feature points on an image frame and track them in the successive frames. For this purpose, the method introduces AKAZE which is a strong feature point detector.

2.2. **Finding a matching area.** Although the Lucas-Kanade (LK) tracker is widely used in the field of target tracking, its application to feature matching is relatively limited. Having detected feature points on one image, it is necessary to search for the matching area on the other image to find the feature point pair. The LK tracker is then used to find the matching area.

2.3. **Feature point matching.** The matching area is obtained by employing the LK tracker. The next step is to achieve feature point matching. The most used algorithms are the brute force (BF) algorithm and the approximate nearest neighbor (ANN) search algorithm. The BF algorithm calculates the distance between a feature descriptor and all other descriptors, and chooses the descriptor having the smallest distance to obtain matched points. The FLANN algorithm adopts a nearest neighbor search. Since the BF algorithm judges the point match according only to the distance between the descriptors, it easily causes a mismatch problem. So the FLANN algorithm is used to complete the feature matching.

3. **Estimation of Human Walking Posture.** Human walking posture is estimated by the rotational motion of a camera worn by a person. Epipolar geometry is taken into account for this purpose [9,22].

Using the geometric relationship between two images, the relative motion relationship between two camera positions is obtained. The relative motion of the camera is used to obtain the change of human walking posture. The epipolar geometry depends on the intrinsic parameters of the cameras as well as their relative poses. We calibrate the intrinsic parameters of the camera in advance to obtain the relative motion of the camera. In order to obtain the relative motion of the camera more accurately, we use RANSAC and bundle adjustment to obtain an essential matrix. The rotation matrix can be calculated from the essential matrix. The rotation matrix is decomposed into three rotation matrices around each axis and the rotation angles are calculated.

Let us denote the corresponding points in the two images as $\boldsymbol{p} = [x, y, z]^{\mathrm{T}}$ and $\boldsymbol{p'} = [x', y', z']^{\mathrm{T}}$. The relationship between the two points $\boldsymbol{p}$ and $\boldsymbol{p'}$ and the fundamental matrix $\boldsymbol{F}$ is given by $\boldsymbol{p'}^{\mathrm{T}}\boldsymbol{F}\boldsymbol{p} = 0$, and the relationship between the fundamental matrix and the essential matrix is provided by $\boldsymbol{F} = \boldsymbol{K}^{-\mathrm{T}}\boldsymbol{E}\boldsymbol{K}^{-1}$, where $\boldsymbol{K}$ is the camera intrinsic parameter matrix. Then we have the following expression:

$$\boldsymbol{p'}\boldsymbol{K}^{-\mathrm{T}}\boldsymbol{E}\boldsymbol{K}^{-1}\boldsymbol{p} = 0 \tag{1}$$

$$\boldsymbol{q'}^{\mathrm{T}}\boldsymbol{E}\boldsymbol{q} = 0 \tag{2}$$

Here $\boldsymbol{q}$ and $\boldsymbol{q'}$ are the corresponding points in the normalized images. The essential matrix $\boldsymbol{E}$ is calculated from the 5-point algorithm [23] using RANSAC.

3.1. **Calculation of a rotation matrix.** The essential matrix consists of the rotation matrix and the translation vector. Using singular value decomposition (SVD), the rotation matrix is calculated by the constraints of the 3-D point cloud in front of the camera. Using bundle adjustment [24] to improve the precision of the 3-D point cloud and camera orientation, we obtain the rotation matrix that fits the observed feature points best when the point cloud is re-projected onto the image.

3.2. **Calculation of rotation angles.** The camera coordinate system is shown in Figure 2, the horizontal direction is the x-axis (pitch), the vertical direction is the y-axis (yaw), and the forward direction is the z-axis (roll). Obtained rotation matrix $\boldsymbol{R}$ is further decomposed into three rotation matrices around the three axes (pitch, yaw, roll) as follows:

$$\boldsymbol{R} = \boldsymbol{R}_r\boldsymbol{R}_p\boldsymbol{R}_y = \begin{bmatrix} r_{11} & r_{12} & r_{13} \\ r_{21} & r_{22} & r_{23} \\ r_{31} & r_{32} & r_{33} \end{bmatrix} \tag{3}$$

$$\boldsymbol{R}_p = \begin{bmatrix} 1 & 0 & 0 \\ 0 & \cos\theta_p & -\sin\theta_p \\ 0 & \sin\theta_p & \cos\theta_p \end{bmatrix} \tag{4}$$

$$\boldsymbol{R}_y = \begin{bmatrix} \cos\theta_y & 0 & \sin\theta_y \\ 0 & 1 & 0 \\ -\sin\theta_y & 0 & \cos\theta_y \end{bmatrix} \tag{5}$$

$$\boldsymbol{R}_r = \begin{bmatrix} \cos\theta_r & -\sin\theta_r & 0 \\ \sin\theta_r & \cos\theta_r & 0 \\ 0 & 0 & 1 \end{bmatrix} \tag{6}$$

Here θ_p, θ_y and θ_r are pitch, yaw and roll angles, respectively.

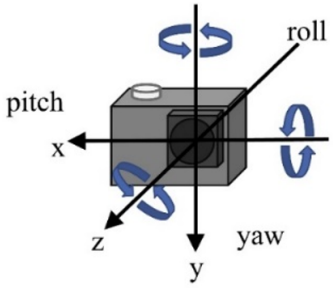

FIGURE 2. The camera coordinate system

The rotation angle around each axis is given by

$$\theta_p = \sin^{-1} r_{32}, \quad \theta_y = -\tan^{-1} \frac{r_{31}}{r_{33}}, \quad \theta_r = -\tan^{-1} \frac{r_{12}}{r_{22}} \tag{7}$$

The device we use is a wearable camera, and the change in human body posture drives the movement of the camera. The pitch/yaw/roll rotation angle of the camera reflects the pitch/yaw/roll rotation change of the human walking posture. Therefore, we analyze the obtained rotation angles as the posture of the human body.

4. **Analysis of Human Walking Posture.** Using the method introduced in the previous section, two consecutive images of a walking motion are chosen and the relative camera motion between the two images is calculated (See Figure 3 for the case of a normal walking motion). Due to the instability and irregularity of the waveform, the processing of a human walking posture waveform is relatively complicated, and it is difficult to analyze the internal relationship directly from it. We do some processing on the waveform to get a regular waveform for subsequent analysis. The obtained waveforms of the rotation angles will have an overall offset. The calculation stated in the previous section is for the relative rotation transformation between the two images. This means that, after continuous calculation, there will be accumulated errors in the waveform. They should be eliminated from the waveform before calculating the indicators of human walking posture.

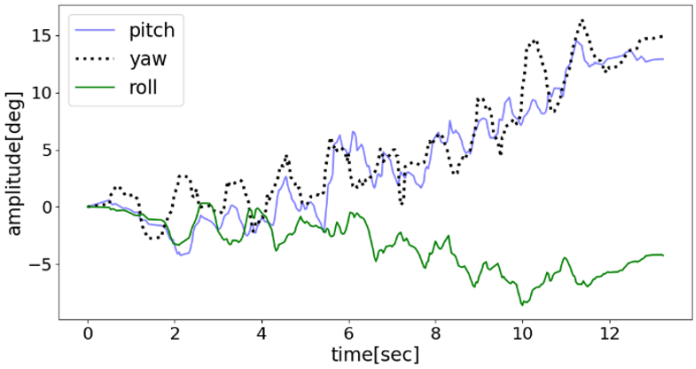

FIGURE 3. Calculated angles (The case of normal walk)

4.1. **Elimination of accumulated errors.** Detrending is performed to remove the accumulated errors of the obtained walking waveform. Detrending can eliminate the impact of offsets generated when acquiring data on later calculation. Removing trends from data allows the analysis to focus only on fluctuations in the data trends. The principle of detrending is to eliminate the trend changes in the data by subtracting a fitted straight line, as shown in Figure 4, from the dot plot image of the original data. This method

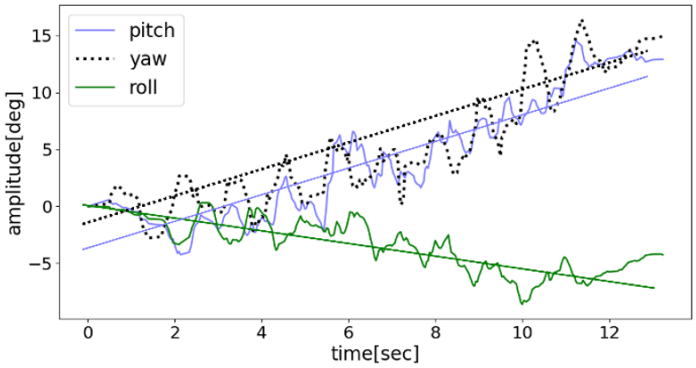

FIGURE 4. Trend changes in the data (The case of normal walk)

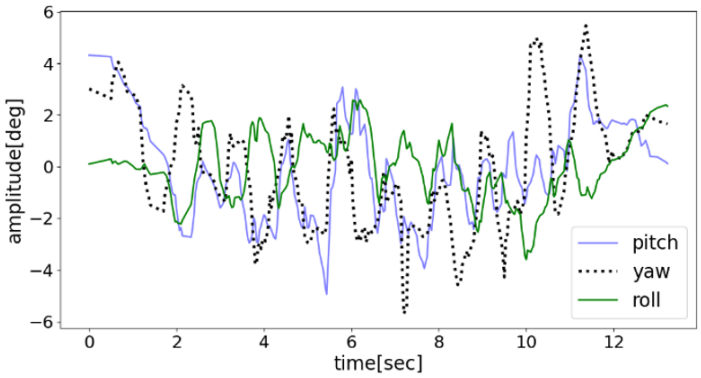

FIGURE 5. Estimated values after detrending (The case of normal walk)

can get the fluctuation characteristics of the waveform. The fitting curve of the image trend is obtained by the least square method, and the ordinate value under the corresponding abscissa of the obtained fitting curve is subtracted from the ordinate value of the corresponding point, which is the detrended image given in Figure 5.

As shown in Figure 5 after detrending, the initial angle of the waveform is generally not 0, and the values at both ends of the waveform do not match, resulting in discontinuity in the Fourier transform. In general, when performing Fourier transform on an unsmooth or discontinuous waveform, its spectrum is scattered in a wide range from low frequency to high frequency, and many additional spectra will appear besides the original frequency. Therefore, in the proposed method, the waveform of the detrended walking posture is transformed approximately to 0 at both ends of the waveform based on the humming window described by

$$g(x) = \begin{cases} 0.54 - 0.46\cos 2\pi x, & \text{if } a \le x \le b \\ 0, & \text{otherwise} \end{cases} \tag{8}$$

Application of Equation (8) to the waveform shown in Figure 5 produces the waveform in Figure 6. The expansion of the base is slightly larger due to the remaining discontinuities. On the other hand, the peaks are sharper and are characterized by higher frequency resolution. Then Fourier transform is performed to the waveform in Figure 6 to get the maximum amplitude spectrum and to find the extremums of the waveform with respect to the frequency as shown in Figure 7. Using the results, we get the extremums of the human walking posture waveform as shown in Figure 8.

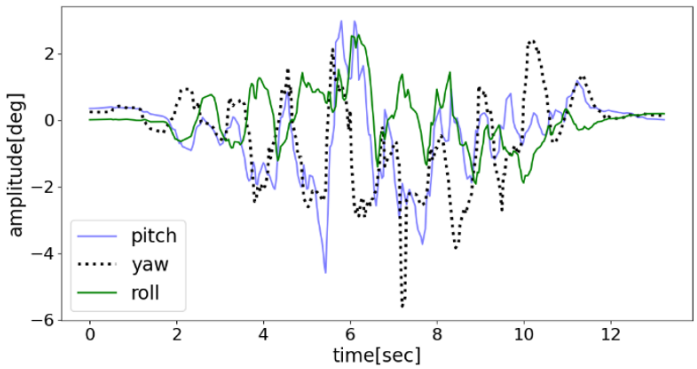

FIGURE 6. Estimated values after applying the humming window (The case of normal walk)

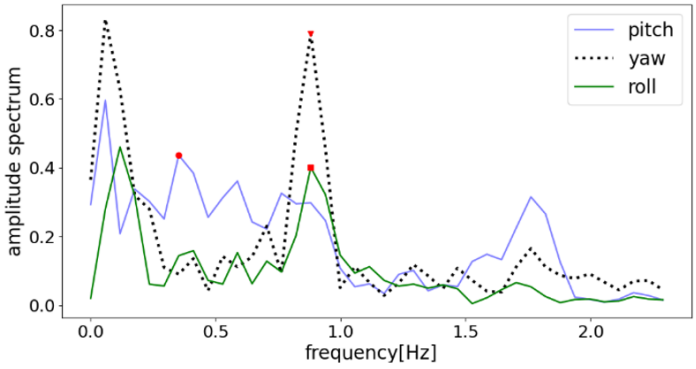

FIGURE 7. Estimated rotation angle frequency (The case of normal walk)

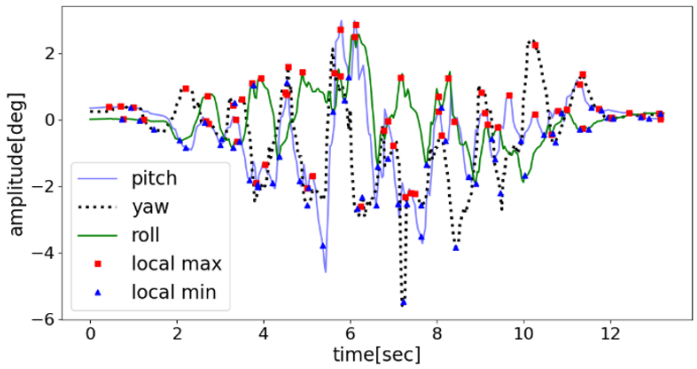

FIGURE 8. The extremums (The case of normal walk)

4.2. **Indicators of human walking posture.** The adjacent extremums are used to obtain the swing angle φ_i of the human walking cycle and the inclination angle ρ_i of the walking human body. These indicators are mainly used to prevent falls of the elderly. They can also be used to know the changes in the balance ability of the spine and lower limbs caused by small changes in posture during the recovery period of postoperative personnel. Through the analysis of these indicators, the problems of walking posture are understood and the walking posture is expected to improve. The definitions of the indicators are given as follows:

$$\varphi_i = a_i - b_i, \quad i = 1, 2, \ldots, N \tag{9}$$

$$\rho_i = \frac{a_i + b_i}{2}, \quad i = 1, 2, \ldots, N \tag{10}$$

$$\bar{\varphi} = \frac{1}{N}(\varphi_1 + \varphi_2 + \cdots + \varphi_N) \tag{11}$$

$$\bar{\rho} = \frac{1}{N}(\rho_1 + \rho_2 + \cdots + \rho_N) \tag{12}$$

Here, a_i is the local maximum, b_i is the local minimum and N is the number of extremums. $\bar{\varphi}$ is the average value of the swing angles and $\bar{\rho}$ is the average value of the inclination angles.

5. **Experimental Results.** In this section, some experimental results are shown and quantitative analysis of the proposed method is conducted for human walking posture estimation to verify the feasibility of the proposed method. In addition, the analysis is performed on the scenes of the same person, multiple postures, and multiple locations.

5.1. **Verification of feasibility.** Normally, the change of human walking posture will not exceed the rotation range of ±30[deg]. So, we use a robotic arm control device as shown in Figure 9(a) to control the rotation around the pitch/yaw/roll axis from 0[deg], to 30[deg], to 0[deg], to −30[deg] and to 0[deg] continuously. The movement of the robot arm is shown in Table 1.

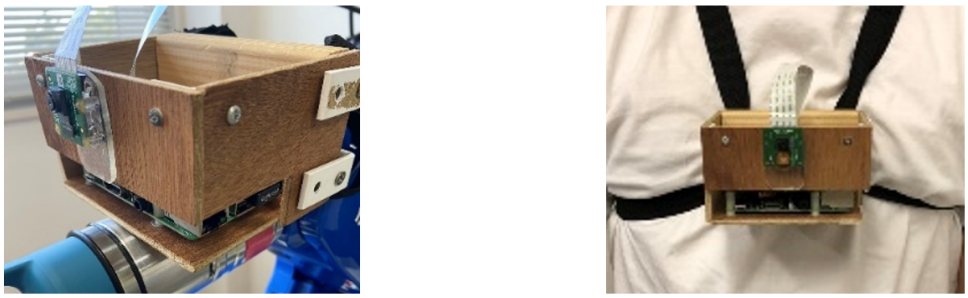

(a) Wearing state on the robotic arm (b) Wearing state on the human body

FIGURE 9. Experimental scenery of the sensor box

TABLE 1. Robot arm movement around each rotation axis

Rotation axis / Rotation range	Pitch (The x-axis rotation)	Yaw (The y-axis rotation)	Roll (The z-axis rotation)
From 0[deg] to 30[deg]	Robot arm rotates around the x-axis upward.	Robot arm rotates around the y-axis to the right.	Robot arm rotates around the z-axis clockwise.
From 0[deg] to −30[deg]	Robot arm rotates around the x-axis downward.	Robot arm rotates around the y-axis to the left.	Robot arm rotates around the z-axis counter-clockwise.

From Table 1, we can find that the rotation around the x-axis (pitch) stands for the robot arm (or a human trunk) which bends backward/forward, and the rotation around the y-axis (yaw) stands for the robot arm/human trunk which rotates to the right/left, whereas the z-axis (roll) means the robot arm/human trunk rotation clockwise/counter-clockwise.

Using the proposed method, the variation in walking posture for each axis is obtained. For experimental comparison, we use a multi-axis sensor to acquire sensor data while

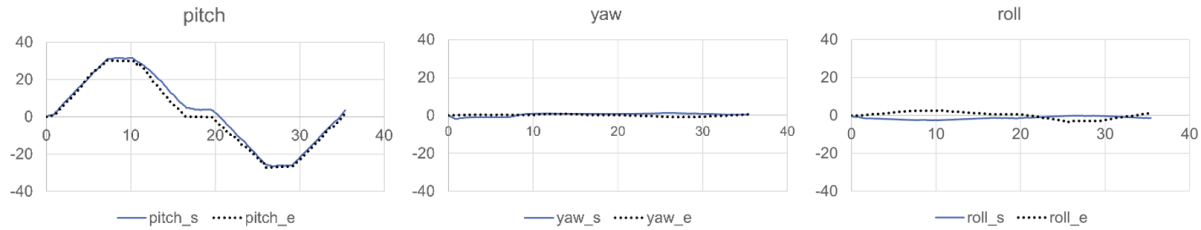

(a) Rotation around the pitch axis from 0[deg], to 30[deg], to 0[deg], to −30[deg] and to 0[deg]

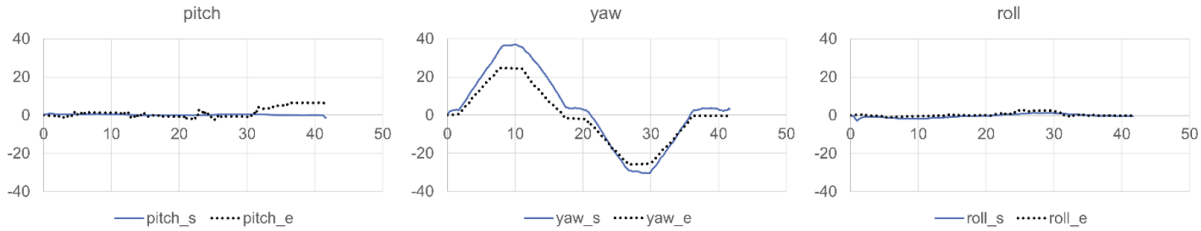

(b) Rotation around the yaw axis from 0[deg], to 30[deg], to 0[deg], to −30[deg] and to 0[deg]

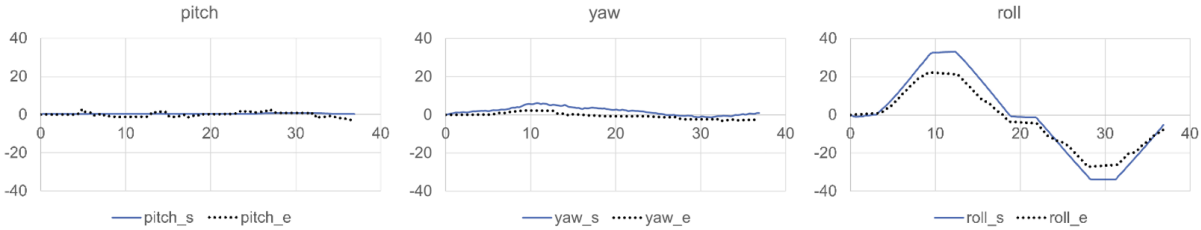

(c) Rotation around the roll axis from 0[deg], to 30[deg], to 0[deg], to −30[deg] and to 0[deg]
(pitch_s, yaw_s, roll_s are the sensor values; pitch_e, yaw_e, roll_e are the estimated values.)

FIGURE 10. The results of estimation of the angle and the sensor angle (The horizontal axis is time [s], and the vertical axis is angle [deg].)

the camera is shooting. The angle in the initial state is set to 0[deg], and the rotation angle of the sensor relative to the initial state is estimated by integration. The errors are calculated as the difference between the rotation angle acquired by the sensor and the real rotation angle of the robot arm. The result is shown in Figure 10.

When rotating around the pitch axis, the roll and yaw axes are nearly 0[deg]. The accuracy is the same when the rotation of the pitch axis is 30[deg] and −30[deg], and when it is 0[deg], the estimation method is more accurate than the multi-axis sensor.

When rotating around the yaw axis, the pitch and roll axes are nearly 0[deg]. When the rotation of the yaw axis is 30[deg], the error between the estimation method and the multi-axis sensor is the same, and when the rotation is −30[deg], the multi-axis sensor has good accuracy. However, at the last 0[deg], the estimation method is more accurate than the multi-axis sensor.

When rotating around the roll axis, the pitch and yaw axes are nearly 0[deg]. When the rotation of the roll axis is 30[deg], the accuracy of the multi-axis sensor is good, and the estimation method and the multi-axis sensor have the same accuracy at −30[deg].

By comparing the error of the proposed estimation method with the multi-axis sensor, the proposed method is almost the same as the sensor or more accurate than the sensor. We confirmed the effectiveness of the estimation method through the experiment using a robot arm.

5.2. **Analysis of the walking postures.** We use a camera worn by a person as shown in Figure 9(b) to get video data each of whose frame has 640×480 pixels and the frame rate is 30.00 fps. In the experiment, four kinds of walking postures, i.e., 'normal walk', 'left shoulder down walk', 'right foot drag walk', and 'bend walk' were taken videos at three different locations (place A, B and C) as given in Figure 11, that amounts to 12 videos. The details of the videos are shown in Table 2. Figure 12 depicts the experimental data of different walking motions at place A. The analysis is done with respect to the four different walking motions of the same subject at three different places.

(a) Place A (b) Place B (c) Place C

FIGURE 11. Experimental locations

TABLE 2. Experimental video details

Walk motion / Place	Normal walk	Left shoulder down walk	Right foot drag walk	Bend walk
A	571 frames	602 frames	1382 frames	754 frames
B	425 frames	451 frames	782 frames	633 frames
C	366 frames	423 frames	871 frames	483 frames

Using the proposed method, we obtain the waveforms of human walking posture as given in Figure 13. We find that the angle range of each axis is about ± 4[deg] for normal walk (Figure 13(a)). For walk motion 1, the overall waveform is shifted downward, especially the pitch and roll axes are below 0[deg] most of the time (Figure 13(b)). For walk motion 2, the fluctuation range of each axis is very large (Figure 13(c)). For walk motion 3, it is similar to walk motion 1, and the overall waveform is shifted downward and the pitch axis is below 0[deg] most of the time (Figure 13(d)).

The obtained walking motion waveform includes the sections before and after walking. Considering the reliability and the stability of the walking motion, the extremum values at the beginning and the ending 3 seconds were removed. The average values $\bar{P}_{l\_\max}$, $\bar{P}_{l\_\min}$, $\bar{Y}_{l\_\max}$, $\bar{Y}_{l\_\min}$, $\bar{R}_{l\_\max}$, $\bar{R}_{l\_\min}$ of the local maximum values and the local minimum values with each axis are calculated as follows:

$$\bar{P}_{l\_\max} = \frac{1}{N}\sum_{i=1}^{N} a_{i_p}, \quad \bar{P}_{l\_\min} = \frac{1}{N}\sum_{i=1}^{N} b_{i_p} \tag{13}$$

$$\bar{Y}_{l\_\max} = \frac{1}{N}\sum_{i=1}^{N} a_{i_y}, \quad \bar{Y}_{l\_\min} = \frac{1}{N}\sum_{i=1}^{N} b_{i_y} \tag{14}$$

$$\bar{R}_{l\_\max} = \frac{1}{N}\sum_{i=1}^{N} a_{i_r}, \quad \bar{R}_{l\_\min} = \frac{1}{N}\sum_{i=1}^{N} b_{i_r} \tag{15}$$

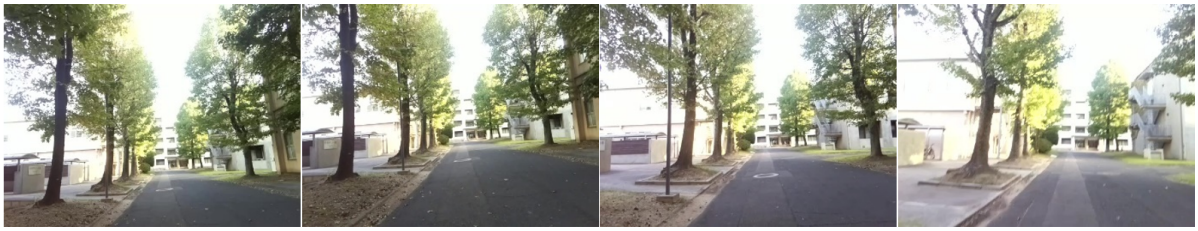

(a) Normal walk

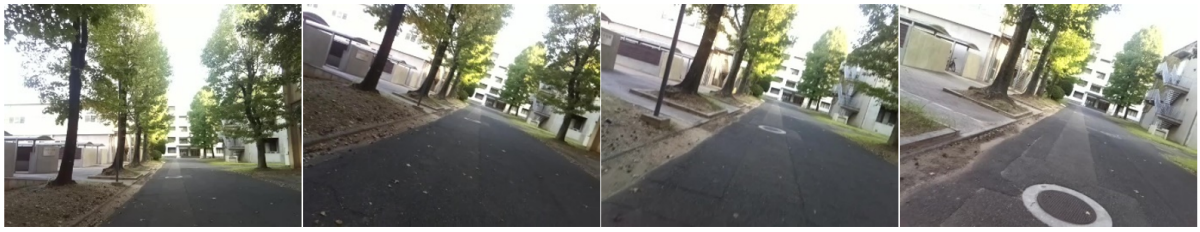

(b) Left shoulder down walk

(c) Right foot drag walk

(d) Bend walk

FIGURE 12. Examples of walking motions obtained from a wearable camera at place A

The obtained averaged swing angles $\bar{\varphi}_p$, $\bar{\varphi}_y$, $\bar{\varphi}_r$ of the human walking cycle and the averaged inclination angles $\bar{\rho}_p$, $\bar{\rho}_y$, $\bar{\rho}_r$ of the walking human body are given in Table 3.

Usually bend walking causes the body to lean forward, which means $\bar{P}_{l\_\max}$, $\bar{P}_{l\_\min}$, $\bar{\rho}_p$ will get smaller. Because of the foot problem, the whole body is not well balanced. This means that $\bar{\varphi}_p$, $\bar{\varphi}_y$, $\bar{\varphi}_r$ will be quite large. Human body leaning to the left and right is mainly reflected in $\bar{R}_{l\_\max}$, $\bar{R}_{l\_\min}$, $\bar{\rho}_r$.

Comparing the walk motion 1 with the normal walk, $\left(\bar{P}_{l\_\max}, \bar{P}_{l\_\min}\right)$ changed from $(0.927, -0.439)$ to $(-0.844, -1.566)$, $\left(\bar{R}_{l\_\max}, \bar{R}_{l\_\min}\right)$ changed from $(0.337, -0.683)$ to $(-0.808, -1.506)$, the average values of the extremums with the pitch and roll axes are significantly smaller. There is no change in the swing angles, but the inclination angles with the pitch and roll axes $(\bar{\rho}_p, \bar{\rho}_r)$ become $(-1.205, -1.157)$. The walk motion 1 is similar to bend walk, because the pitch axis is inclined downward. The larger the inclination of the roll axis means the body trunk is tilted to the right, and the smaller the inclination of the roll axis means the body trunk is tilted to the left. So, there is a high

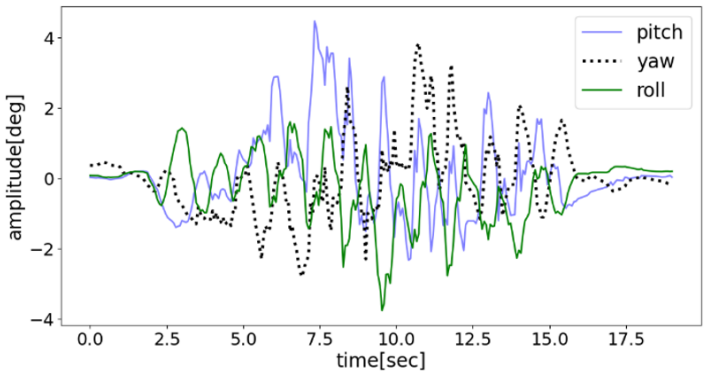

(a) Normal walk

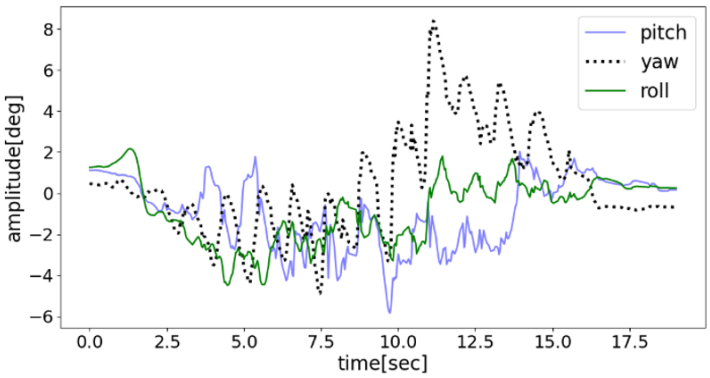

(b) Walk motion 1: Left shoulder down walk

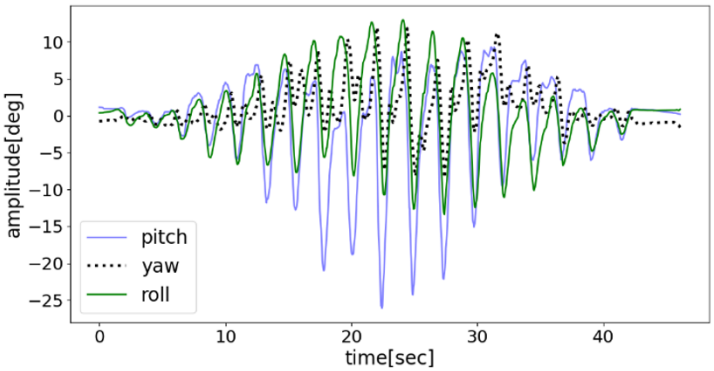

(c) Walk motion 2: Right foot drag walk

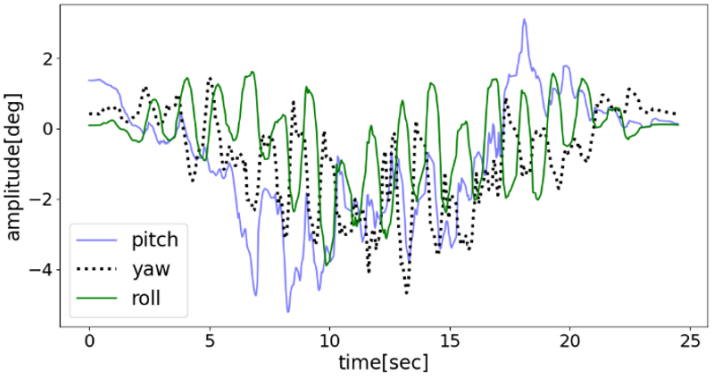

(d) Walk motion 3: Bend walk

FIGURE 13. The waveform of human walking postures at place A

TABLE 3. The indicators about the human walking postures at place A

	Normal walk	Walk motion 1	Walk motion 2	Walk motion 3
$\bar{P}_{l\_\max}$[deg]	0.927	−0.844	4.243	−0.787
$\bar{P}_{l\_\min}$[deg]	−0.439	−1.566	−4.630	−1.621
$\bar{Y}_{l\_\max}$[deg]	1.032	1.527	3.193	−0.730
$\bar{Y}_{l\_\min}$[deg]	0.245	−0.336	−1.037	−1.780
$\bar{R}_{l\_\max}$[deg]	0.337	−0.808	5.355	0.640
$\bar{R}_{l\_\min}$[deg]	−0.683	−1.506	−6.465	−1.271
$\bar{\varphi}_p$[deg]	1.366	0.722	8.873	0.834
$\bar{\varphi}_y$[deg]	0.787	1.863	4.230	1.050
$\bar{\varphi}_r$[deg]	1.020	0.698	11.82	1.911
$\bar{\rho}_p$[deg]	0.244	−1.205	−0.194	−1.204
$\bar{\rho}_y$[deg]	0.639	0.600	1.078	−1.255
$\bar{\rho}_r$[deg]	−0.173	−1.157	−0.555	−0.316

possibility that the motion is left shoulder down walk. On the other hand, with the walk motion 2 compared with the normal walk, the swing angles $(\bar{\varphi}_p, \bar{\varphi}_y, \bar{\varphi}_r)$ is very large that is $(8.873, 4.230, 11.82)$. It can be concluded that the balance of this motion is very poor, and it can be inferred that it is caused by leg problems. So, the walk motion 2 is concluded as right foot drag walk. The average value of the extremums with the pitch axes and the inclination angle with the pitch axis $\left(\bar{P}_{l\_\max}, \bar{P}_{l\_\min}, \bar{\rho}_p\right)$ become $(-0.787, -1.621, -1.204)$ in the walk motion 3, because the pitch axis is inclined downward. Therefore the walk motion 3 is regarded as bend walk.

For the place B and C, we got the same conclusion by comparison. The human walking motion predicted by the quantitative analysis of the indicators is consistent with the real walking motion.

6. **Discussion.** In this paper, we proposed a method of human walking posture estimation and analysis using a wearable camera. As was shown in Figure 10, the movement of the three rotations can be clearly inferred, since the rotations around two axes are almost zero compared with the other rotation. In the case of pitch axis (yaw axis) rotation, the up and down (left and right) motion of the screen allows better feature points tracking using LK tracker. This improves the quality of points correspondence. On the other hand, the screen produces a rotational movement around the roll axis, and the feature points tracking is harder in the area distant from the image center. This will make the quality of corresponding points degrade and has an adverse effect on the calculation of 3D points. Fortunately, when a human walks, the rotation around the roll axis is not large normally and relatively high-quality corresponding points can be obtained.

Feature points extraction by AKAZE works well, since the scale rotation is invariant and it has good robustness in lighting and other situations. However, only in the case of bend walking, the view of the ego camera almost captures the road, and it is difficult to extract the feature points on the road surface well. The overall number of corresponding points then decreases, which affects the estimation accuracy negatively. This difficulty may be solved by focusing on road surface texture using a high-precision camera at the expense of cost or by developing a stronger feature point detector.

7. **Conclusion.** This paper proposed a method of estimating and analyzing a human walking posture for the purpose of discovering a physical problem in a body and improving posture. The algorithm of the estimation and analysis was presented and the performance of the method was shown by the experiment using a normal walking motion and three biased walking motions. Unlike the existent methods which deal with human posture analysis using cameras set around a person, the proposed method performs the analysis based on the video taken from a camera worn by the person. This means that the proposed method employs the video of a scene in front of the person the worn camera takes, whereas the existent methods employ the video of a human itself. The idea of analyzing the frontal scene comes from the fact that unusual change in the frontal scene suggests a certain physical change of the camera wearer.

Focusing the attention on human walk motion, the present paper described how the method estimates and analyzes characteristic walking posture automatically. The performance of the method was shown by the experiment and satisfactory results were obtained for future practical use. The result is expecting for deepening the study. Future topics include the improvement of the estimation accuracy of human walking posture and adding further indicators for more detailed human posture analysis, other than increasing experimental data.

The present method has opened the study on human motion analysis from indoor observation to even outdoor observation by use of a wearable camera. The method can analyze human walking posture collected at any place, irrespective of indoors or outdoors. In the near future, the present study may propose a system realizing daily check of ego posture of a walker by hanging a cool ego camera around one's neck.

Acknowledgment. This work was supported by JSPS KAKENHI Grant Number 16K01 554.

REFERENCES

[1] R. Nakamura, H. Saito and H. Nagasaki, *Fundamental Kinesiology*, Ishiyaku Publishers, 2012.
[2] C. A. Oatis, *Kinesiology: The Mechanics and Pathomechanics of Human Movement*, Lippincott Williams & Wilkins, 2009.
[3] S. D. Glassman, K. Bridwell, J. R. Dimar, W. Horton, S. Berven and F. Schwab, The impact of positive sagittal balance in adult spinal deformity, *Spine*, vol.30, no.18, pp.2024-2029, 2005.
[4] D. Saha, S. Gard and S. Fatone, The effect of trunk flexion on able-bodied gait, *Gait & Posture*, vol.27, no.4, pp.653-660, 2008.
[5] L. Z. Rubenstein, Falls in older people: Epidemiology, risk factors and strategies for prevention, *Age and Ageing*, vol.35, no.suppl_2, pp.37-41, 2006.
[6] S. Leteneur, C. Gillet, H. Sadeghi, P. Allard and F. Barbier, Effect of trunk inclination on lower limb joint and lumbar moments in able men during the stance phase of gait, *Clinical Biomechanics*, vol.24, no.2, pp.190-195, 2009.
[7] M. J. Mathie, A. C. F. Coster, N. H. Lovell and B. G. Celler, Accelerometry: Providing an integrated, practical method for long-term, ambulatory monitoring of human movement, *Physiological Measurement*, vol.25, no.2, R1-20, 2004.
[8] S. Ishikawa, J. K. Tan, H. Kim and S. Ishikawa, 3-D recovery of a non-rigid object from a single camera view by piecewise recovery and synthesis, *Proc. of the 21st Int. Conf. on Pattern Recognition*, pp.1443-1446, 2012.
[9] Z. Liu, T. Chihara and J. K. Tan, Ego-posture estimation for a pedestrian using a monocular wearable camera, *ICCCS*, pp.409-412, 2020.
[10] B. Bodenheimer, C. Rose, S. Rosenthal and J. Pella, The process of motion capture: Dealing with the data, *Computer Animation and Simulation'97*, pp.3-18, 1997.
[11] T. Shiratori, H. S. Park, L. Sigal, Y. Sheikh and J. K. Hodgins, Motion capture from body-mounted cameras, *ACM Trans. Graphics*, vol.30, no.2, pp.1-10, 2011.

[12] X. Jiang and M. Tamagawa, Effect of falling down postures on human injuries by multi-body dynamic simulation using OpenSim, *ICIC Express Letters, Part B: Applications*, vol.12, no.12, pp.1121-1128, 2021.
[13] B. Sapp, A. Toshev and B. Taskar, Cascaded models for articulated pose estimation, *European Conference on Computer Vision*, pp.406-420, 2010.
[14] X. Zhang, C. Li, X. Tong, W. Hu, S. Maybank and Y. Zhang, Efficient human pose estimation via parsing a tree structure based human model, *IEEE*, pp.1349-1356, 2009.
[15] Z. Cao, T. Simon, S. E. Wei and Y. Sheikh, Realtime multi-person 2D pose estimation using part affinity fields, *arXiv.org*, arXiv: 1611.08050, 2017.
[16] D. Mehta, S. Sridhar, O. Sotnychenko, H. Rhodin, M. Shafiei, H. P. Seidel, W. Xu, D. Casas and C. Theobalt, VNect: Real-time 3D human pose estimation with a single RGB camera, *ACM Trans. Graphics (TOG)*, vol.36, no.4, article no.44, 2017.
[17] S. Benenaula, M. D. Trelles, L. E. Garza-Castañón and L. I. Minchala, Classification of gait anomalies by using space-time parameters obtained with pose estimation, *International Journal of Innovative Computing, Information and Control*, vol.18, no.6, pp.1913-1927, 2022.
[18] J. K. Tan and T. Kurosaki, Estimation of self-posture of a pedestrian using MY VISION based on depth and motion network, *Journal of Robotics, Networking and Artificial Life*, vol.7, no.3, pp.152-155, 2020.
[19] D. G. Lowe, Distinctive image features from scale-invariant keypoints, *International Journal of Computer Vision*, vol.60, pp.91-110, 2004.
[20] H. Bay, T. Tuytelaars and L. Van Gool, SURF: Speeded up robust features, *European Conference on Computer Vision*, pp.404-417, 2006.
[21] P. F. Alcantarilla, A. Bartoli and A. J. Davison, KAZE features, *European Conference on Computer Vision*, pp.214-227, 2012.
[22] Z. Liu, T. Kurosaki and J. K. Tan, Recognition of human walking motion using a wearable camera, *International Conference on Computing and Pattern Recognition (ICCPR)*, 2022.
[23] D. Nistér, An efficient solution to the five-point relative pose problem, *IEEE Trans. Pattern Analysis and Machine Intelligence*, vol.26, no.6, pp.756-770, 2004.
[24] S. Gratton, A. S. Lawless and N. K. Nichols, Approximate Gauss-Newton methods for nonlinear least squares problems, *SIAM Journal on Optimization*, vol.18, no.1, pp.106-132, 2007.

Author Biography

Ziyue Liu received B.E. degree in Mechanical Design, Manufacturing and Automation in 2014 from the School of Mechanical and Electrical Engineering, University of Electronic Science and Technology of China. He received M.E. degree in Control Engineering in 2020 from Faculty of Engineering, Kyushu Institute of Technology, Japan. His research interests are image processing, pattern recognition, and robotics.

Joo Kooi Tan received the Ph.D. degree from Kyushu Institute of Technology. She is currently a professor with the Department of Mechanical and Control Engineering, Kyushu Institute of Technology. Her current research interests include ego-motion analysis by MY VISION, three-dimensional shape/motion recovery, human detection, and its motion analysis from video. She was awarded SICE Kyushu Branch Young Author's Award in 1999, the AROB Young Author's Award in 2004, the Young Author's Award from IPSJ of Kyushu Branch in 2004, and the BMFSA Best Paper Award in 2008, 2010, 2013 and 2015. She is a member of IEEE, The Information Processing Society, The Institute of Electronics, Information and Communication Engineers, and The Biomedical Fuzzy Systems Association of Japan.